FINITE ELEMENT MODELING OF THE FRICTION STIR WELDING (FSW) PROCESS OF DISSIMILAR ALUMINUM ALLOYS

Dan Birsan[1]

[1] *"Dunarea de Jos" University of Galati, dbirsan@ugal.ro.*

Abstract: *Friction Stir Welding (FSW) is a solid-state joining technique widely used for high-strength aluminum alloys, offering clear advantages over conventional fusion welding. Among dissimilar combinations, the joint between AA7075 and AA6061-T6 has gained increasing interest due to its applications in aerospace, automotive, marine, and defense industries, where lightweight and high-performance structures are required. This study develops a finite element model (FEM) to simulate the thermo-mechanical behavior of the FSW process in these alloys. The model accounts for tool geometry, rotational and traverse speeds, and material constitutive laws to predict temperature distribution, plastic flow, strain evolution, and residual stresses. Validation against experimental data ensures the accuracy and reliability of the simulations. The results confirm that the solid-state nature of FSW minimizes defects typical of fusion welding, such as porosity, hot cracking, and shrinkage. Dissimilar joints produced by FSW show superior fatigue resistance, higher tensile strength retention, and improved microstructural stability. Additionally, the process generates lower heat input, reducing distortion and preserving desirable properties, while eliminating the need for filler materials or shielding gases, thus lowering cost and environmental impact. Overall, the FEM framework provides valuable insights into material flow and thermal history, supporting process optimization and confirming FSW as a robust solution for advanced engineering applications.*

Keywords: *FSW, finite element, stress, strain*

1. Introduction

Friction Stir Welding (FSW) is a solid-state joining process that enables the fabrication of defect-free welds in high-strength aluminum alloys through intense plastic deformation and frictional heating. The dissimilar combination of AA7075, known for its high strength-to-weight ratio, and AA6061-T6, valued for its excellent corrosion resistance and weldability, offers a balance of mechanical performance and durability. Such joints are increasingly employed in aerospace fuselage and wing structures, automotive frames, marine vessels, and defense components, where weight reduction and structural integrity are of primary importance.

As shown in Ref. [1], the authors demonstrated that combining machine learning models with finite element simulations provides a reliable framework for optimizing FSW parameters in steel joints, identifying feasible process windows despite the limited dataset. Gradient Boosting Regressor (R^2 = 0.69) and Artificial Neural Networks (R^2 = 0.70) achieved the best predictive performance, showing the potential of data-driven approaches to support industrial adoption of FSW in shipbuilding.

Wan and co. [2] established a multi-physical field coupled finite element model to

investigate the wear behavior of stirring tools in friction stir welding. Their results showed that selecting optimal welding parameters, particularly a rotational speed of 840 rpm and a travel speed of 180 mm/min, reduced tool wear by 97.9% compared to less favorable conditions, significantly extending tool life and ensuring process reliability.

The authors [3] analyzed the performance of blind rivet joints made from different materials and subjected to various loading conditions. They concluded that stainless steel rivets combined with double-lap shear configurations provided the highest strength and most reliable joint performance.

Ye and co. [4] investigated the effect of interference-fit tolerance and installation speed on the mechanical behavior of CFRP/Al blind riveted joints. They found that an optimal interference of about 0.42% significantly enhanced joint strength, highlighting the importance of process parameter optimization for reliable performance.

The authors [5] demonstrated that applying intermittent ultrasonic vibration at optimal parameters significantly improved the mechanical performance of FSW T-joints, achieving higher yield strength, tensile strength, and elongation. Furthermore, the proposed constitutive model, implemented in ABAQUS, accurately predicted the creep behavior of the joints, showing excellent agreement with experimental results.

2. Finite-element modeling

The proposed numerical model enables a detailed investigation of the mechanisms occurring during joint formation, as well as the interaction between the tool between the plates. To ensure accuracy, the outcomes of the finite element analysis must be validated either through experimental comparison or by benchmarking against results available in the literature. For the simulation of the FSW process, the study employed Simufact Forming software (Simufact Engineering GmbH, Hamburg, Germany), using a coupled thermo-mechanical approach to evaluate temperature evolution, material deformation, and stress distribution throughout the joining procedure.

Table 1: *Chemical compositions*

	Al	Mg	Si	Fe	Cu	Cr	Zn	Ti
AA7075	87.1 91.4	2.1 2.9	0 0.4	0 0.5	1.2 2.0	0.18 0.28	5.1 6.1	0 0.2
AA6061	95.8 98.6	0.8 1.2	0.4 0.8	<= 0.7	0.15 0.4	0.04 0.35	<= 0.25	<= 0.15

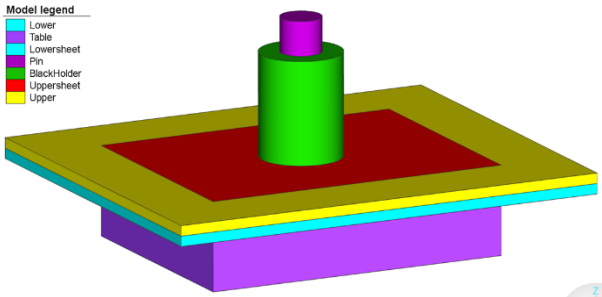

Figure 1: *Finite-element model*

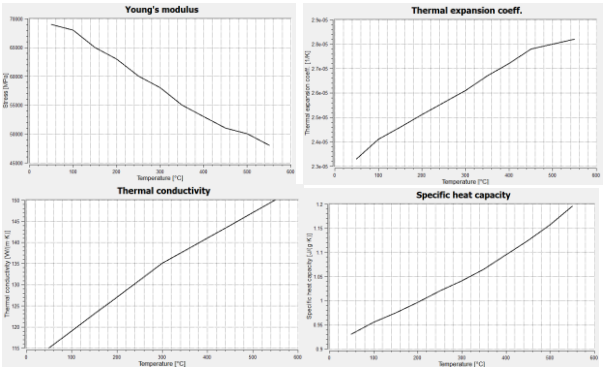

The following equation represents the mathematical model of the material behaviour:

$$\sigma_F = C_1 \cdot e^{(C_2 \cdot T)} \cdot \varepsilon_p^{(n_1 \cdot T + n_2)} \cdot e^{\left(\frac{l_1 \cdot T + l_2}{\varphi}\right)} \cdot \dot{\varepsilon}_p^{(m_1 \cdot T + m_2)}$$

Mat.	C1	C2	l1	l2	m1	m2	n1	n2
AA 6061-T6	405.9	-0.0032	-4.344e-5	0.01674	3.731e-4	-0.05181	-5.610e-5	0.2530
AA 7075-T6	506.5	-0.0044	5.756e-5	-0.0280	2.659e-4	-0.00110	-4.818e-5	-0.1061

The finite element model included the workpieces, the welding tool, and the supporting table, as illustrated in Figure 1. To eliminate any degrees of freedom, the lower surface of the bottom plate was fully constrained. In order to approximate real experimental conditions, several simplifications were introduced without compromising accuracy: 2D elements for axisymmetric analysis, identified in Simufact

Forming as Quad (10). A total of 2380 elements were used to represent the top and bottom plates, while the welding tool and support structures were modeled as rigid components, discretized with 5020 quadratic Quad elements. The finite element model was designed to simulate the friction stir welding of two aluminum alloy plates with a thickness of 1.5 mm each. The welding tool was represented by a cylindrical pin with a diameter of 5 mm, modeled as a rigid body, while the plates were treated as deformable bodies discretized with structured quadrilateral elements to ensure accurate resolution of thermo-mechanical gradients. Rotational speed was varied from 2000 to 2400 rpm in steps of 100 rpm, and plunge depth ranged between 1.2 mm and 1.4 mm with an increment of 0.5 mm.

Boundary conditions were applied by fully constraining the lower surface of the bottom plate, while tool rotation and translational movement were imposed as kinematic inputs. A surface-to-surface contact algorithm with a frictional formulation was used to describe the interaction between the tool and the plates, ensuring the transfer of heat and mechanical loads. Adaptive remeshing was employed to account for large plastic deformations in the stir zone. These modeling assumptions enabled the evaluation of temperature distribution, strain accumulation, and potential defect formation under varying process parameters.

3. Results and Discussions

Table 2 summarizes the finite element analysis results concerning the peak temperature and residual stress levels under different FSW process parameters. The dataset considers variations in pin penetration depth and tool rotational speed. The findings highlight the sensitivity of thermal and mechanical responses of the joints to these parameters, indicating that higher tool speeds and deeper pin penetration tend to increase the maximum temperature, while residual stress outcomes depend on the complex interaction of all process variables.

Table 2: *Temperature and residual stress from finite element analysis*

No.	Depth [mm]	Speed [rpm]	$T_{max.}$ [°C]	Residual stress [MPa]
1	1.2	1800	381	241
2		1900	387	238
3		2000	395	233
4		2100	403	230
5		2200	414	228
6	1.25	1800	364	245
7		1900	383	240
8		2000	390	236
9		2100	397	233
10		2200	412	226
11	1.3	1800	391	257
12		1900	410	252
13		2000	416	240
14		2100	421	235
15		2200	430	226
16	1.35	1800	362	237
17		1900	375	232
18		2000	383	226
19		2100	395	224
20		2200	407	222
21	1.4	1800	380	223
22		1900	389	234
23		2000	402	230
24		2100	411	228
25		2200	420	223

Fig. 2 illustrates the temperature distribution obtained from the finite element simulation of the Friction Spot Welding process. The welding tool penetrates the overlapping plates, generating heat through friction and plastic deformation. The color scale indicates temperatures ranging from ambient (~20 °C) to approximately 360 °C at the tool–workpiece interface.

The highest temperature zone is localized around the tool pin tip and shoulder, where frictional contact and severe plastic deformation are most intense. This thermal concentration promotes material softening and enables effective mixing in the stir zone. The temperature gradually decreases away from the weld center, as indicated by the transition from

red to dark blue, demonstrating the expected heat dissipation into the surrounding material.
The simulation confirms that heat generation is highly localized at the tool–workpiece interface, ensuring sufficient plasticization for bonding while limiting excessive thermal exposure in adjacent regions. This controlled temperature field is essential for avoiding defects such as porosity, cracking, or distortion, and contributes to the formation of a sound joint.

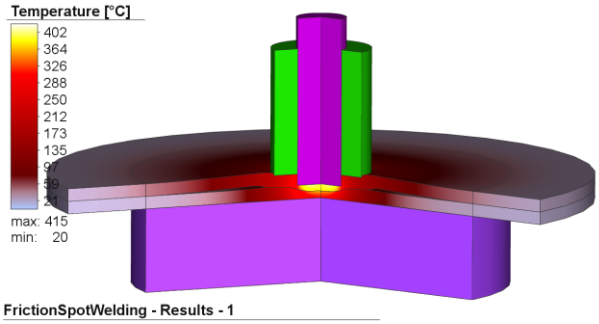

Figure 2: *Temperature at the end of the process case 23*

The graph, Fig.3, illustrates the variation of maximum temperature in the upper sheet as a function of time during the FSW process. The temperature rises rapidly in the first second due to intense frictional heating and plastic deformation, followed by a gradual increase up to a peak of approximately 360 °C at around 4.2 seconds. After reaching this maximum, the curve shows a sharp decline, indicating the cooling phase once the tool rotation and penetration are completed. This profile highlights the transient thermal cycle characteristic of FSW, where controlled heat generation is essential for material softening, joint formation, and defect avoidance.

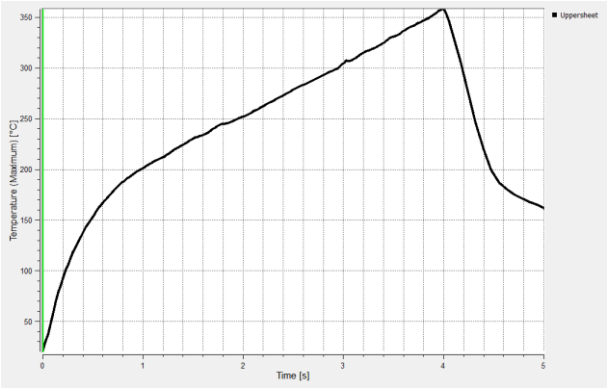

Figure 3: *Temperature evolution during FSW process*

Fig. 4 displays the equivalent stress distribution during the Friction Spot Welding process, obtained through finite element simulation. The maximum stresses, approaching 528 MPa, are concentrated around the tool–workpiece interface, particularly near the pin and shoulder contact zone. This is consistent with the regions experiencing the most intense plastic deformation and load transfer during the plunging stage.
The stress field gradually decreases radially away from the weld center, as indicated by the color gradient from red/yellow (high stress) to blue (low stress). The base plates remain at lower stress levels (<100 MPa), confirming that the mechanical load is highly localized around the stir zone and does not induce significant residual stresses in the outer regions.
The stress gradient is steep, showing efficient confinement of deformation in the weld region. Limited stress propagation into the plates suggests reduced risk of distortion or large-scale cracking.
The results validate that process parameters are within safe limits to achieve bonding without excessive damage to surrounding material.

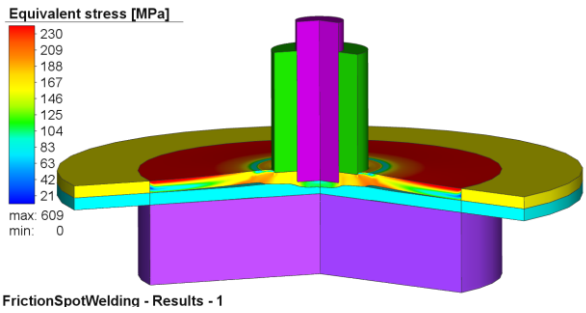

Figure 4: *Equivalent stress at the end of the process*

The graph, Fig.5, shows the variation of equivalent stress (MPa) as a function of time (s) during the FSW process. At the beginning, the stress level peaks at nearly 250 MPa, corresponding to the tool plunging stage when material resistance is highest. As the process continues, the stress decreases steadily due to material softening caused by frictional heating and plastic flow.

After about 3.5–4 seconds, the stress drops more sharply, reflecting the completion of tool penetration and the onset of the holding/retraction stage. By the end of the cycle, the stress stabilizes at a low value, indicating reduced load transfer once the material has been sufficiently plasticized and the tool is withdrawn.

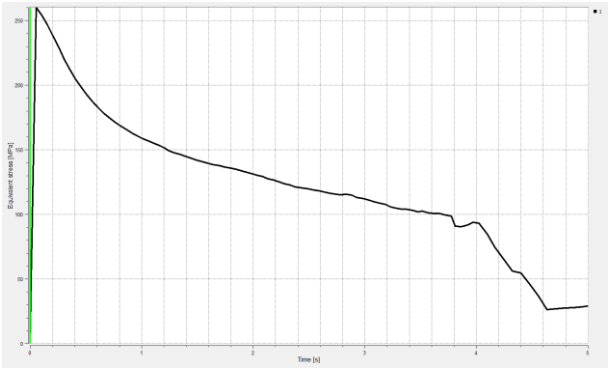

Figure 5: *Equivalent stress evolution during FSW process*

4. Conclusions

This research analyzes the influence of key welding parameters—namely plunge depth, rotational speed, and welding duration—on the performance of RFSSW joints in dissimilar materials. After initial trials, welding tests were performed using boundary values of the selected input factors. The results can be summarized as follows:

Thermal analysis confirmed that the peak temperatures within the stir zone (SZ) remained well below the melting point of aluminum, thereby verifying the solid-state character of the process. The temperature cycles measured on the tool axis showed a close correlation and evolution patterns similar to those in the literature.

Residual stress evaluation, based on finite element modeling, revealed substantial stresses within the stir zone and thermo-mechanically affected zone (TMAZ), arising mainly from thermal gradients and localized plastic strain. Nevertheless, these stresses were consistently lower than the yield strength of the parent alloy, indicating a minimized risk of crack initiation when process parameters are properly controlled.

References

1. [Panfiglio, 2025] Panfiglio S., Chairi M., Denaro A., Marabello G., Borsellino C., Di Bella G., *Optimization of friction stir welding parameters for steel joints in shipbuilding using machine learning and finite element analysis,* Materials Research Proceedings 54, 2025.
2. [Wan, 2025] Wan Q., Wang S., *Research On The Influence Of Welding Parameters Of FSW On Stirring Tool Wear*, Journal of Applied Science and Engineering, Vol. 28, No 11 the Institution of Mechanical Engineers, Part B: Journal of Engineering Manufacture, SAGE, 2025.
3. [Brooks, 2025] Brooks K., Ramos B., Prymak D., Nelson T, Miles M., *Improving Simulation Model Accuracy for Friction Stir Welding of AA 2219*, Materials, 2025.
4. [Ye, 2025] Ye T., Han Y., Zuo D., Fu H., Feng S., Gao C., Li W., *Research on Creep Deformation of Dissimilar FSWed T-Joints Under Different Ultrasonic Vibration Modes: Experiment, Constitutive Model, and Simulation Verification*, Materials, 2025.
5. [Khokhlov, 2025] Khokhlov M.A., Kostin V.A., Khokhlova J.A., PoklaytskiyA.G., Makhnenko O.O., *Modeling of temperature fields distribution and stress-strain state of Mg-Al alloy FSW joints*, Welding and Related Technologies, 2025.
6. [Toumi, 2024] Toumi F., Benyounes H., Khelfaoui Y., *Thermomechanical Analysis and Microstructural Characterization of AA7075-T6 Lap Joints Produced by FSW*, Metals, MDPI, 2024.
7. [Delgado, 2024] Delgado I., Martínez J., Ruiz P., *Detection of Defects in FSW AA7075-T6 Joints Using Computed Tomography*, Journal of Nondestructive Evaluation, Taylor & Francis, 2024.
8. [Di Bella, 2023] Di Bella G., Russo F., Lombardo M., *Review of Process Parameters and Defect Formation in Friction Stir Welding of Aluminum Alloys*, Metals, MDPI, 2023.
9. [Dewangan, 2023] Dewangan R., Yadav S., Patel R., *Finite Element Simulation and Experimental Validation of Temperature Distribution in AA7075 FSW*, Physica B: Condensed Matter, Elsevier, 2023.
10. [Ansari, 2023] Ansari A., Kumar V., Singh R., *Finite Element Modeling Framework for Coupled Thermo-Mechanical Analysis of FSW*, Preprint (NSF Registered), 2023.

11. [Review, 2023] Anonymous, *Numerical Modeling of Friction Stir Welding and Processing: Advances and Applications*, Open Access Review, 2023.
12. [Ghiasvand, 2022a] Ghiasvand A., Heidarpour A., Afshar A., *Numerical and Experimental Investigation of Tool Positioning Effects on Peak Temperature in Dissimilar AA6061-T6/AA7075-T6 FSW*, Materials, MDPI, 2022.
13. [Ghiasvand, 2022b] Ghiasvand A., Heidarpour A., Afshar A., *Effect of Tool Positioning on Ultimate Tensile Strength in AA6061-T6/AA7075-T6 Dissimilar FSW*, Materials, MDPI, 2022.
14. [Kaewkham, 2022] Kaewkham P., Chaichana C., Somkiat K., *Improvement of Mechanical Properties in Dissimilar AA6061-T6/AA7075-T651 Friction Stir Welding*, 2022.
15. [Vasu, 2022] Vasu A., Shanmuganathan S., *Three-Dimensional Finite Element Simulation of Transient Temperature Distribution in FSW of AA6061 and AA7075*, International Journal of Engineering Research & Technology, 2022.
16. [***, 2019] ***, *Simufact Forming Theory manual*. Champaign. Computational Applications and System Integration Inc., 2019.